

A general framework for knowledge integration in machine learning for electromagnetic scattering using quasinormal modes

Viktor A. Lilja, Albin J. Svärdsby, Timo Gahlmann, and Philippe Tassin
Department of Physics, Chalmers University of Technology, SE-41296 Göteborg, Sweden
 (Dated: September 9, 2025)

Neural networks have been demonstrated to be able to provide fast surrogate models that can accelerate the inverse design of optical and electromagnetic devices. Nevertheless, such neural networks can be unreliable and normally require extreme amounts of data for training. Here we show that these limitations can be alleviated by constraining neural-network models using prior knowledge about the governing physics. We propose a universal physics-informed neural network for electromagnetic scattering based on the quasinormal mode expansion of the scattering matrix. Our neural-network model learns the resonant structure underlying the scattering spectrum and is guaranteed to obey energy conservation and causality. We demonstrate significantly improved data efficiency for photonic-crystal slabs and all-dielectric free-form metasurfaces. The method can be applied to a wide range of optical and electromagnetic devices owing to the generality of the quasinormal mode formalism.

Machine learning [1, 2] is a powerful tool for inverse design in electromagnetism, mechanics, materials science, quantum many-body systems, and other paradigms of physics [3–13]. The goal of inverse design is to find a device design that exhibits some predefined properties [14–18]. For linear electromagnetic devices, the properties are often quantities that describe the relation between incoming and outgoing amplitudes of electromagnetic waves, such as transmittance, reflectance, or absorption [5–7, 13, 17–37]. These quantities can be derived from the frequency-dependent scattering matrix $S(\omega)$, which encodes the complete scattering response of a general linear N -port device [38]. The forward problem of finding $S(\omega)$ for a given design can be solved with full-wave electrodynamics solvers. The inverse problem is more difficult as it requires searching through the vast space of possible designs. One solution is to replace the simulator with a neural network (NN) trained to predict $S(\omega)$ given a design parametrization, summarized schematically as

$$\text{Design} \xrightarrow{\text{NN}} S(\omega).$$

Once trained, this forward model can typically predict $S(\omega)$ orders of magnitude faster than an electrodynamics solver. This allows for efficient exploration of the design space through iterative optimization [18, 39] or the training of inverse models [21, 29–32, 36, 40]. The downside of this approach is that the performance of the final design becomes dependent on the accuracy of the NN. Although it may be possible to improve accuracy by increasing the number of trainable parameters and the number of training samples, computational resources are often a limiting factor. Furthermore, the black box nature of NNs makes them unreliable and very limited insights can be gained from their predictions [41].

These issues can be alleviated by utilizing prior knowledge about the governing physics [41, 42], a strategy often referred to as physics-informed machine learn-

ing. One physics-informed method, which has recently gathered attention in electromagnetic scattering problems [13, 19, 24, 28], is to include a physics layer as a final step in the forward model. The augmented forward model can be schematically summarized as

$$\text{Design} \xrightarrow{\text{NN}} \begin{matrix} \text{Physics} \\ \text{parameters} \end{matrix} \xrightarrow{\text{Physics model}} S(\omega), \quad (1)$$

where the physics model is a known computable expression for $S(\omega)$ with the physics parameters as arguments. Now, any constraints imposed on the physics model will also be satisfied by the full forward model. Furthermore, the task of the NN has become to predict the physics parameters rather than $S(\omega)$ directly, which may be easier to learn. Indeed, previous works have demonstrated that using a physics layer reduces prediction error for a given NN size [13, 24, 28], improves generalization [19, 24, 28], and reduces the required amount of training data [19, 28]. Another benefit is that the physics parameters become accessible as a learned latent description [19, 28] that can be used as a design target in the inverse problem [13]. The forward model also becomes less of a black box in the sense that the predicted spectra can be explained in terms of the physics parameters. Implementing the physics model in a numerical framework that supports automatic differentiation enables the full forward model to be trained directly on simulated $S(\omega)$. This is in contrast to the methods proposed in Refs. [27, 39, 43–45], where the physics parameters are extracted from $S(\omega)$ before training.

Various physics models that exploit the resonant structure of the scattering matrix have been proposed in the literature [13, 24, 28], but are either tailored to specific device geometries [13, 28] or rely on spectral decompositions without a formal theoretical basis [24]. However, the general and exact relation between resonances and scattering parameters is, in fact, known and is formalized by the theory of quasinormal modes (QNMs) [46, 47]. We

propose a physics-informed NN architecture based on the QNM expansion of the scattering matrix. We will refer to this architecture as the QNM-Net. Owing to the generality of the QNM formalism, the QNM-Net is universal in the sense that it can be applied to devices with an arbitrary number of resonances and scattering ports. Furthermore, the rich physics of the QNM formalism allows us to impose strong constraints on the physics model to improve accuracy and data efficiency.

QNMs are a generalization of normal modes to lossy systems. They are defined as eigenmodes of the source-free Maxwell's equations

$$\begin{aligned}\nabla \times \tilde{\mathbf{E}}_m &= i\tilde{\omega}_m \mu \tilde{\mathbf{H}}_m \\ \nabla \times \tilde{\mathbf{H}}_m &= -i\tilde{\omega}_m \varepsilon \tilde{\mathbf{E}}_m\end{aligned}\quad (2)$$

with outgoing radiation boundary conditions, where $\tilde{\omega}_m$ is the QNM eigenfrequency and m enumerates the QNMs. Due to the open boundary and material absorption, the eigenproblem is non-Hermitian and $\tilde{\omega}_m = \omega_m + i\gamma_m$ complex-valued. The imaginary part γ_m corresponds to a decay in time and can be decomposed as $\gamma_m = \gamma_{r,m} + \gamma_{nr,m}$, where $\gamma_{r,m}$ is due to radiative losses and $\gamma_{nr,m}$ is due to nonradiative losses [48, 49].

A connection can be made between $S(\omega)$ and the QNMs by expanding the scattered electromagnetic field as a sum of the QNM fields $\tilde{\mathbf{E}}_m$ and $\tilde{\mathbf{H}}_m$ [46, 47, 50]. This so-called quasinormal mode expansion of the scattering matrix makes it clear that the QNM frequencies $\tilde{\omega}_m$ correspond to resonances in the scattering spectrum, as illustrated in Fig. 1. Many different versions of the expansion can be found in the literature [46, 47, 50, 51]. In this work, we use the form

$$S(\omega) = e^{i\omega\tau} [C(\omega) + D(i\omega - i\tilde{\Omega})^{-1} M^{-1} D^\dagger C(\omega)] e^{i\omega\tau}, \quad (3)$$

which is approximate but specifically formulated to respect energy conservation even when a finite number of QNMs are included in the expansion [51], making it suitable for our application. In this expression, for an N -port device with P modes, $C(\omega)$ is an $N \times N$ matrix representing a slowly varying background, D is an $N \times P$ matrix with columns \mathbf{d}_m , $\tilde{\Omega}$ is a diagonal matrix of QNM frequencies $\tilde{\omega}_m$, and M is a $P \times P$ matrix with elements

$$M_{mp} = \frac{\mathbf{d}_m^\dagger \mathbf{d}_p}{i\tilde{\omega}_{r,p} - i\tilde{\omega}_{r,m}^*},$$

where $\tilde{\omega}_{r,m} = \omega_m + i\gamma_{r,m}$. The N complex-valued elements of \mathbf{d}_m should be interpreted as the amplitudes of the m :th QNM on the ports. Finally, τ is a diagonal $N \times N$ matrix of real numbers τ_n that determine the phase accumulated between the scatterer and the ports. We refer to Ref. [51] for a more in-depth description, derivation and error analysis.

Our proposed physics-informed NN architecture incorporates the QNM-expansion as a physics model according

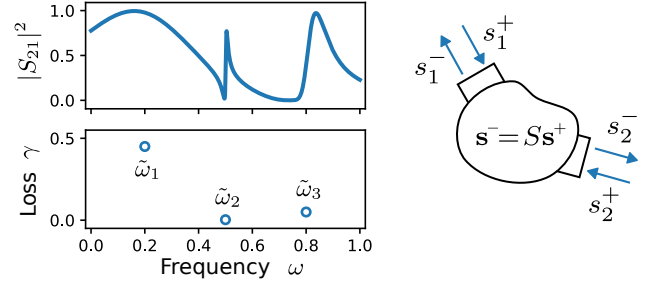


FIG. 1. Relation between the S matrix and QNMs of a fictitious 2-port scattering device. Right: The scattering matrix S relates the amplitudes s_n^\pm of incoming (+) and outgoing (−) waves. Top left: Resonances are observed when plotting elements of S as a function of frequency. Bottom left: Each resonance corresponds to a complex pole of $S(\omega)$. The poles are eigenfrequencies $\tilde{\omega}_m$ of QNMs.

to the principle shown in schematic (1). The physics parameters are in our case $C(\omega)$ and τ , as well as $\tilde{\omega}_m$ and \mathbf{d}_m for each mode m . The architecture is composed of multiple submodels as illustrated in Fig. 2. The first submodel maps the design description to an abstract feature vector φ . The subsequent submodels use φ to predict the physics parameters evaluated at frequency ω . Finally, $S(\omega)$ is computed from the physics parameters using the QNM expansion (3).

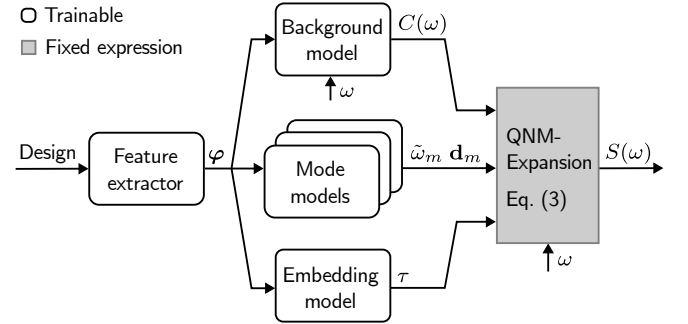


FIG. 2. Overview of the QNM-Net architecture. White boxes are submodels with trainable parameters, the gray box is a fixed analytical physics model. Arrows indicate the relations between inputs and outputs of each submodel.

We demonstrate the QNM-Net on two example systems. The first example is a photonic crystal (PhC) slab, consisting of a sheet of lossless dielectric with a repeating pattern of holes. We study transmission and reflection at normal incidence. The design is described by five parameters (h, r_1, r_2, r_3, r_4) as illustrated in Fig. 3(a). Four-fold rotational symmetry is enforced to ensure polarization independence, resulting in a S matrix of size 2×2 . The scattering spectrum in the frequency range of interest is dominated by a single Fano resonance, as exemplified in Fig. 3(b).

We tailor the QNM-Net implementation to this sys-

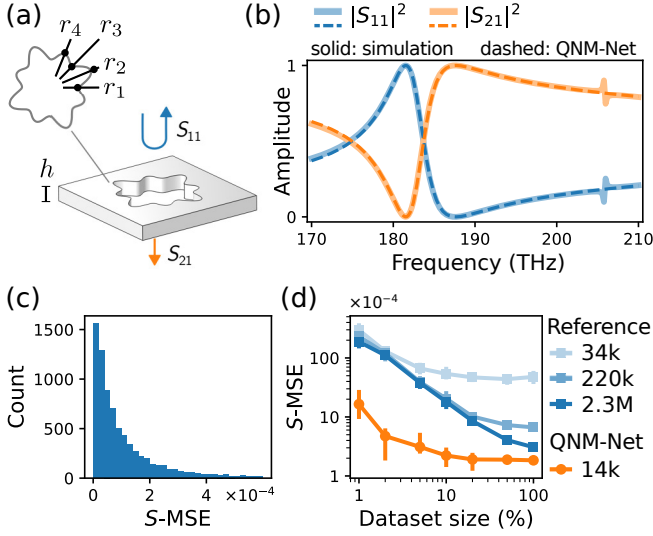


FIG. 3. Applying the QNM-Net to PhC slabs. (a) Illustration of the PhC parametrization and geometry. (b) Simulated and QNM-Net-predicted S parameters for a sample from the validation set. (c) Histogram of test losses for the QNM-Net when using 20% of the dataset. (d) Validation loss as a function of dataset size for the QNM-Net and standard NNs. Markers show cross-validation average, vertical bars show lowest and highest values. Numbers in the legend refer to the number of trainable parameters.

tem by imposing as strong constraints as possible to each of the submodels using problem-specific prior knowledge. The feature extractor consists of a fully-connected feed-forward NN and contains the bulk of the trainable weights. A linear skip connection was added to improve training robustness and convergence speed [13]. Consulting the diagram in Fig. 2, the background model should take φ and ω as inputs and return the corresponding background matrix $C(\omega)$. Because the PhC is reciprocal, lossless, and mirror symmetric, C satisfies $C^T = C$, $C^\dagger C = I$, and $C_{11} = C_{22}$ [51], so we set

$$C = \begin{pmatrix} i \sin \alpha & \cos \alpha \\ \cos \alpha & i \sin \alpha \end{pmatrix} e^{i\alpha}. \quad (4)$$

To allow for a design-dependent slow variation with frequency, we let $\alpha = \alpha(\omega)$ be a linear function of ω with values at 170 THz and 210 THz predicted from φ using a single-layer NN. The mode models should predict the QNM frequencies $\tilde{\omega}_m$ and port amplitudes \mathbf{d}_m from φ , with each mode model corresponding to one mode in the QNM expansion. Because the PhC scattering spectrum is well approximated by a single resonance, we only use one mode model in this case. Furthermore, because the PhC is mirror symmetric, the QNMs are either even or odd, corresponding to $\mathbf{d}_m = (1, 1)$ or $\mathbf{d}_m = (1, -1)$, respectively [46, 51]. The observed Fano mode is even, so we set $\mathbf{d}_1 = (1, 1)$. The material of the PhC being lossless implies $\gamma_{nr,1} = 0$. The remaining unknown and

design-dependent mode parameters ω_1 and $\gamma_{r,1}$ are predicted from φ using a single-layer NN. Causality is enforced by applying a strictly positive activation function to $\gamma_{r,1}$ [51]. Finally, the embedding model should predict τ_n from φ . We use a single-layer NN to predict τ_1 from φ and set $\tau_2 = \tau_1$ because of mirror symmetry.

To train the QNM-Net, we generated a dataset of 10 000 random PhC designs and their corresponding scattering spectra $S(\omega)$ at 200 equally spaced frequency points using frequency-domain finite-element method simulations. The QNM-Net was trained to minimize the S -parameter mean-squared-error (S -MSE), defined as

$$S\text{-MSE} = \frac{1}{N_S N_\omega} \sum_{i,j,k} |S_{ij}^{\text{predicted}}(\omega_k) - S_{ij}^{\text{true}}(\omega_k)|^2,$$

where N_S is the number of elements S_{ij} in the scattering matrix and N_ω is the number of sampled frequencies ω_k . Models were trained on 80% of the dataset while the remaining 20% was used for validation. The validation error was averaged over five dataset splits.

The trained QNM-Net is able to reproduce the simulated scattering accurately, as exemplified by the sample shown in Fig. 3(b). The sample has an S -MSE of 2.1×10^{-4} , which is close to the mean of the loss histogram shown in Fig. 3(c). The histogram was evaluated on a test set separate from both validation and training to avoid bias. For reference, we compare the QNM-Net to three standard fully-connected feed-forward NNs with varying numbers of trainable parameters. Similar architectures have been used in forward models in the literature [18, 21, 22, 26, 36]. Figure 3(d) shows the validation loss for all models at different dataset sizes. The QNM-Net requires only 2% of the dataset, corresponding to 160 training samples, to achieve an S -MSE less than 10^{-3} . The reference models require approximately one order of magnitude more data and trainable parameters to achieve a similar loss. This shows that the QNM-Net can reduce the need for training data significantly by learning the physics of the system in terms of its QNMs. In Appendix A, we verify that the QNM frequencies learned by the network indeed correspond to eigenmodes of the PhC geometry.

To investigate if the QNM-Net approach is also beneficial for more complex geometries when less is known about the physics, we apply the QNM-Net to free-form all-dielectric metasurfaces. We use a dataset introduced in Ref. [52] containing roughly 80 000 meta-atoms and their corresponding scattering spectra. The geometry is described by a 100×100 binary bitmap representing the etching mask for the metasurface unit cell, as illustrated in Fig. 4(a). As far as we know, no previous works have applied NNs with resonance-based physics models to free-form designs. This system has a vastly larger design space, lower frequency resolution, a polarization-dependent scattering response, multiple overlapping resonances, nonradiative loss, and lacks mirror symmetry

due to the presence of a substrate. Furthermore, only two columns of the S matrix, corresponding to light incident from the top, are available in the dataset.

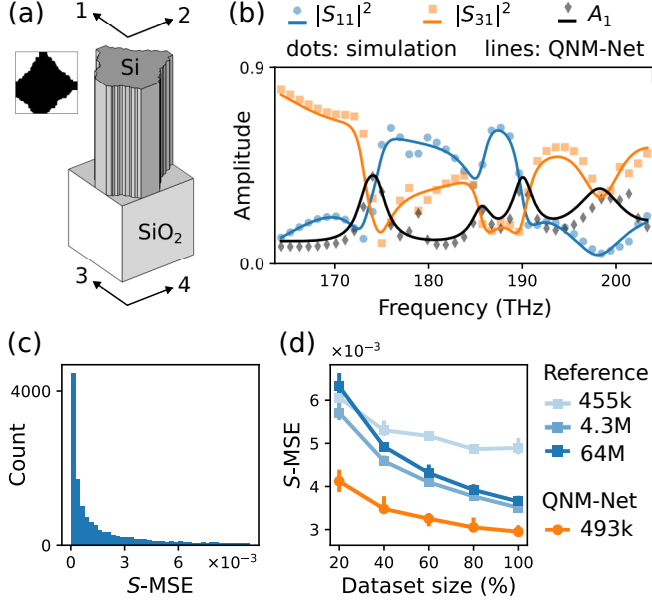


FIG. 4. QNM-Net applied to free-form metasurface. (a) Illustration of a metasurface unit cell and the corresponding bitmap. Numbered arrows indicate the locations and polarizations of the ports. (b) Simulated and QNM-Net-predicted spectrum. $A_1 = 1 - \sum_n |S_{n1}|^2$ is the absorbed power fraction for incidence on port 1. (c) Histogram of QNM-Net test losses for dataset size 80%. (d) Validation loss as a function of dataset size for the QNM-Net and reference models. Numbers in the legend refer to the number of trainable parameters.

We again adapt a QNM-Net architecture based on prior knowledge about the system. Because the design parameterization now has an inherent spatial structure, we use a version of the convolutional DenseNet architecture [53] as the feature extractor, as proposed by Ref. [32]. In this case, there is no clearly distinguishable background. We therefore set $C = -I$, which is commonly used in QNM expansions [46, 51] and let the QNM-Net fit the background using many broad resonances. The spectra have a varying number of modes within the sampled frequency range. We chose to include 20 mode models in the QNM-Net, which we deemed to be sufficient based on manual inspection of a few simulated spectra. If a smaller number of modes are necessary to explain a given spectrum, the QNM-Net can learn to place the superfluous modes outside the sampled range, so that they do not contribute to the predicted spectrum. For each mode, the QNM frequency and damping rates, as well as the real and imaginary parts of \mathbf{d}_m , are predicted from φ by small NNs. Fixed port delays τ_n are used to account for the distance between the metasurface boundary and the ports.

Subsequently, we compare the QNM-Net to reference

models consisting of DenseNets followed by branched feed-forward NNs, similar to the architecture used in Ref. [32]. The same DenseNet architecture was used for all models, but the width of the fully-connected layers was varied to change the number of trainable parameters. Figure 4(b) shows a simulated spectrum and the corresponding QNM-Net prediction for a sample from the validation set. The S -MSE of the prediction is 2.4×10^{-3} , which is typical compared to the histogram shown in Fig. 4(c). We observe that the QNM-Net reproduces most resonances, but fails to predict a few weaker resonances. We believe this is due to the design space being so large that even tens of thousands of training samples are not enough to accurately learn all features of the spectra. Nevertheless, the QNM-Net requires only around one third of the data to achieve a loss as low as that of the best reference models, demonstrating that the method is useful also for this system.

In conclusion, we have demonstrated a modular physics-informed NN architecture for electromagnetic scattering based on the QNM expansion of the scattering matrix. We have shown that this architecture requires significantly less trainable parameters and is substantially more data efficient than conventional NNs. Compared to previous methods, it can be applied to a wider range of systems and it has a more well-founded theoretical basis in the formalism of quasinormal modes. We believe that the method will be useful for modeling a wide range of electromagnetic systems where the scattering spectrum is accurately described by a set of resonances.

The method presented here opens the door to further developments in machine learning for electromagnetic scattering, which previously was limited to overly simplified systems or required an amount of training data that was difficult to obtain in practice. The significantly improved data efficiency can make it practically feasible to train models on experimental data for simple designs. In Appendix B, we demonstrate that the QNM-Net is more robust to noise than standard NNs, which would be advantageous in this scenario. The QNM-Net can also be combined with methods such as those presented in Refs. [54, 55] to account for fabrication-induced performance degradation in inverse design. Furthermore, because the physics parameters learned by the NN have a well-defined connection to electromagnetic eigenmodes, investigating the learned parameters can provide insights into the underlying physics. The rigorous connection to electromagnetic eigenmodes also makes it possible to train the QNM-Net on eigenmode simulations. This approach could be particularly useful for sharp resonances that are not easily resolved in the frequency domain.

ACKNOWLEDGEMENTS

We acknowledge partial financial support from Chalmers' area of advance Nano (Excellence Grant), from the Swedish Research Council under Grant No. 2020-05284, and from the Knut och Alice Wallenberg Stiftelse under Grant No. 2022.0090. Training data generation and NN training were performed on resources provided by the Swedish National Infrastructure for Computing (NAISS), at the Chalmers/C3SE and KTH/PDC sites, partially funded by the Swedish Research Council under Grant No. 2022-06725. The work was performed in part within the framework of the META-PIX Excellence Center META-PIX.

-
- [1] I. N. Da Silva, D. Hernane Spatti, R. Andrade Flauzino, L. H. B. Liboni, and dos Reis Alves, *Artificial Neural Networks: A Practical Course* (Springer, Cham, 2017).
 - [2] B. Mehlig, *Machine Learning with Neural Networks: An Introduction for Scientists and Engineers* (Cambridge University Press, Cambridge, 2021).
 - [3] R. Iten, T. Metger, H. Wilming, L. Del Rio, and R. Renner, Discovering physical concepts with neural networks, *Phys. Rev. Lett.* **124**, 010508 (2020).
 - [4] V. Peano, F. Sapper, and F. Marquardt, Rapid exploration of topological band structures using deep learning, *Phys. Rev. X* **11**, 021052 (2021).
 - [5] P. R. Wiecha, A. Arbouet, C. Girard, and O. L. Muskens, Deep learning in nano-photonics: Inverse design and beyond, *Photonics Res.* **9**, B182 (2021).
 - [6] O. Khatib, S. Ren, J. Malof, and W. J. Padilla, Deep Learning the Electromagnetic Properties of Metamaterials—A Comprehensive Review, *Adv. Funct. Mater.* **31**, 2101748 (2021).
 - [7] J. Jiang, M. Chen, and J. A. Fan, Deep neural networks for the evaluation and design of photonic devices, *Nat. Rev. Mater.* **6**, 679 (2021).
 - [8] M. Zandehshahvar, Y. Kiarashi, M. Chen, R. Barton, and A. Adibi, Inverse design of photonic nanostructures using dimensionality reduction: Reducing the computational complexity, *Opt. Lett.* **46**, 2634 (2021).
 - [9] M. Zandehshahvar, Y. Kiarashinejad, M. Zhu, H. Maleki, T. Brown, and A. Adibi, Manifold learning for knowledge discovery and intelligent inverse design of photonic nanostructures: Breaking the geometric complexity, *ACS Photonics* **9**, 714 (2022).
 - [10] N. Mohseni, T. Fösel, L. Guo, C. Navarrete-Benlloch, and F. Marquardt, Deep learning of quantum many-body dynamics via random driving, *Quantum* **6**, 714 (2022).
 - [11] J. Lee, D. Park, M. Lee, H. Lee, K. Park, I. Lee, and S. Ryu, Machine learning-based inverse design methods considering data characteristics and design space size in materials design and manufacturing: a review, *Mater. Horiz.* **10**, 5436 (2023).
 - [12] M. Sanchez, C. Everly, and P. A. Postigo, Advances in machine learning optimization for classical and quantum photonics, *J. Opt. Soc. Am. B* **41**, A177 (2024).
 - [13] Y. Xu, J.-Q. Yang, K. Fan, S. Wang, J. Wu, C. Zhang, D.-C. Zhan, W. J. Padilla, B. Jin, J. Chen, and P. Wu, Physics-Informed Inverse Design of Programmable Metasurfaces, *Adv. Sci.* **11**, 2406878 (2024).
 - [14] L. Su, D. Vercruysse, J. Skarda, N. V. Sapra, J. A. Petykiewicz, and J. Vučković, Nanophotonic inverse design with SPINS: Software architecture and practical considerations, *Appl. Phys. Rev.* **7**, 011407 (2020).
 - [15] O. Tsilipakos, G. Perrakis, M. Farsari, and M. Kafesaki, Polymeric optical metasurfaces by two-photon lithography: Practical designs for beam steering, in *Metamaterials 2024* (2024) pp. 1–3.
 - [16] R. S. Hegde, Photonics inverse design: pairing deep neural networks with evolutionary algorithms, *IEEE J. Sel. Top. Quantum Electron.* **26**, 1 (2019).
 - [17] S. So, T. Badloe, J. Noh, J. Bravo-Abad, and J. Rho, Deep learning enabled inverse design in nanophotonics, *Nanophotonics* **9**, 1041 (2020).
 - [18] Y. Deng, S. Ren, K. Fan, J. M. Malof, and W. J. Padilla, Neural-adjoint method for the inverse design of all-dielectric metasurfaces, *Opt. Express* **29**, 7526 (2021).
 - [19] Y. Yan, F. Li, J. Shen, M. Zhuang, Y. Gao, W. Chen, Y. Li, Z. Wu, Z. Dong, and J. Zhu, Highly intelligent forward design of metamaterials empowered by circuit-physics-driven deep learning, *Laser Photonics Rev.* **2400724** (2024).
 - [20] C. C. Nadell, B. Huang, J. M. Malof, and W. J. Padilla, Deep learning for accelerated all-dielectric metasurface design, *Opt. Express* **27**, 27523 (2019).
 - [21] S. Sarkar, A. Ji, Z. Jermain, R. Lipton, M. Brongersma, K. Dayal, and H. Y. Noh, Physics-Informed Machine Learning for Inverse Design of Optical Metamaterials, *Adv. Photonics Res.* **4**, 2300158 (2023).
 - [22] L. Xu, M. Rahmani, Y. Ma, D. A. Smirnova, K. Z. Kamali, F. Deng, Y. K. Chiang, L. Huang, H. Zhang, S. Gould, D. N. Neshev, and A. E. Miroshnichenko, Enhanced light-matter interactions in dielectric nanostructures via machine-learning approach, *Adv. Photonics* **2**, 026003 (2020).
 - [23] Y. Jing, H. Chu, B. Huang, J. Luo, W. Wang, and Y. Lai, A deep neural network for general scattering matrix, *Nanophotonics* **12**, 2583 (2023).
 - [24] A.-P. Blanchard-Dionne and O. J. F. Martin, Teaching optics to a machine learning network, *Opt. Lett.* **45**, 2922 (2020).
 - [25] T. Zhang, C. Y. Kee, Y. S. Ang, E. Li, and L. K. Ang, Symmetry Enhanced Network Architecture Search for Complex Metasurface Design, *IEEE Access* **10**, 73533 (2022).
 - [26] S. So, J. Mun, and J. Rho, Simultaneous Inverse Design of Materials and Structures via Deep Learning: Demonstration of Dipole Resonance Engineering Using Core-Shell Nanoparticles, *ACS Appl. Mater. Interfaces* **11**, 24264 (2019).
 - [27] X. Ma, Y. Ma, P. Cunha, Q. Liu, K. Kudtarkar, D. Xu, J. Wang, Y. Chen, Z. J. Wong, M. Liu, M. C. Hipwell, and S. Lan, Strategical Deep Learning for Photonic Bound States in the Continuum, *Laser Photonics Rev.* **16**, 2100658 (2022).
 - [28] O. Khatib, S. Ren, J. Malof, and W. J. Padilla, Learning the Physics of All-Dielectric Metamaterials with Deep Lorentz Neural Networks, *Adv. Opt. Mater.* **10**, 2200097 (2022).
 - [29] W. Ma, F. Cheng, Y. Xu, Q. Wen, and Y. Liu, Probabilistic Representation and Inverse Design of Metamaterials

- Based on a Deep Generative Model with Semi-Supervised Learning Strategy, *Adv. Mater.* **31**, 1901111 (2019).
- [30] Z. Liu, D. Zhu, S. P. Rodrigues, K.-T. Lee, and W. Cai, Generative Model for the Inverse Design of Metasurfaces, *Nano Lett.* **18**, 6570 (2018).
- [31] J. Xu, P. Xu, Z. Yang, F. Liu, L. Xu, J. Lou, B. Fang, and X. Jing, Freeform metasurface design with a conditional generative adversarial network, *Appl. Phys. A* **130**, 530 (2024).
- [32] T. Gahlmann and P. Tassin, Deep neural networks for the prediction of the optical properties and the free-form inverse design of metamaterials, *Phys. Rev. B* **106**, 085408 (2022).
- [33] C. Yeung, B. Pham, R. Tsai, K. T. Fountaine, and A. P. Raman, DeepAdjoint: An All-in-One Photonic Inverse Design Framework Integrating Data-Driven Machine Learning with Optimization Algorithms, *ACS Photonics* **10**, 884 (2023).
- [34] M. H. Tahersima, K. Kojima, T. Koike-Akino, D. Jha, B. Wang, C. Lin, and K. Parsons, Deep Neural Network Inverse Design of Integrated Photonic Power Splitters, *Sci. Rep.* **9**, 1368 (2019).
- [35] Y. Qian, B. Ni, Z. Feng, H. Ni, X. Zhou, L. Yang, and J. Chang, Deep Learning for the Design of Random Coding Metasurfaces, *Plasmonics* **18**, 1941 (2023).
- [36] D. Liu, Y. Tan, E. Khoram, and Z. Yu, Training Deep Neural Networks for the Inverse Design of Nanophotonic Structures, *ACS Photonics* **5**, 1365 (2018).
- [37] G. You, C. Qian, S. Tan, E. Li, and H. Chen, Driving deep-learning-based metasurface design with Kramers-Kronig relations, *Phys. Rev. Appl.* **22**, L041002 (2024).
- [38] R. E. Collin, *Field Theory of Guided Waves* (Wiley-Interscience-IEEE, 1991).
- [39] J. L. Su, J. W. You, L. Chen, X. Y. Yu, Q. C. Yin, G. H. Yuan, S. Q. Huang, Q. Ma, J. N. Zhang, and T. J. Cui, MetaPhyNet: Intelligent design of large-scale metasurfaces based on physics-driven neural network, *J. Phys. Photonics* **6**, 035010 (2024).
- [40] Z. A. Kudyshev, A. V. Kildishev, V. M. Shalaev, and A. Boltasseva, Machine learning-assisted global optimization of photonic devices, *Nanophotonics* **10**, 371 (2021).
- [41] S. W. Kim, I. Kim, J. Lee, and S. Lee, Knowledge Integration into deep learning in dynamical systems: An overview and taxonomy, *J. Mech. Sci. Technol.* **35**, 1331 (2021).
- [42] G. E. Karniadakis, I. G. Kevrekidis, L. Lu, P. Perdikaris, S. Wang, and L. Yang, Physics-informed machine learning, *Nat. Rev. Phys.* **3**, 422 (2021).
- [43] J. Zhang, J. W. You, F. Feng, W. Na, Z. C. Lou, Q.-J. Zhang, and T. J. Cui, Physics-Driven Machine-Learning Approach Incorporating Temporal Coupled Mode Theory for Intelligent Design of Metasurfaces, *IEEE Trans. Microwave Theory Tech.* **71**, 2875 (2023).
- [44] X. Ding, V. Devabhaktuni, B. Chattaraj, M. Yagoub, M. Deo, J. Xu, and Q. J. Zhang, Neural-network approaches to electromagnetic-based modeling of passive components and their applications to high-frequency and high-speed nonlinear circuit optimization, *IEEE Trans. Microwave Theory Tech.* **52**, 436 (2004).
- [45] S. Liu, F. Feng, X. Huang, M. Li, X. Li, J. Liu, W. Liu, and Q.-J. Zhang, Novel Neuro-Coupling Matrix Technique for Parametric Modeling of Microwave Filters, *IEEE Microwave Wireless Technol. Lett.* **34**, 871 (2024).
- [46] F. Alpeggiani, N. Parappurath, E. Verhagen, and L. Kuipers, Quasinormal-Mode Expansion of the Scattering Matrix, *Phys. Rev. X* **7**, 021035 (2017).
- [47] H. Zhang and O. D. Miller, Quasinormal Coupled Mode Theory (2020), [arXiv:2010.08650](https://arxiv.org/abs/2010.08650).
- [48] P. Lalanne, W. Yan, K. Vynck, C. Sauvan, and J.-P. Hugonin, Light Interaction with Photonic and Plasmonic Resonances, *Laser Photonics Rev.* **12**, 1700113 (2018).
- [49] P. T. Kristensen, K. Herrmann, F. Intravaia, and K. Busch, Modeling electromagnetic resonators using quasinormal modes, *Adv. Opt. Photonics* **12**, 612 (2020).
- [50] T. Weiss and E. A. Muljarov, How to calculate the pole expansion of the optical scattering matrix from the resonant states, *Phys. Rev. B* **98**, 085433 (2018).
- [51] M. Benzaouia, J. D. Joannopoulos, S. G. Johnson, and A. Karalis, Quasi-normal mode theory of the scattering matrix, enforcing fundamental constraints for truncated expansions, *Phys. Rev. Res.* **3**, 033228 (2021).
- [52] T. Gahlmann and P. Tassin, Evaluation of machine learning techniques for conditional generative adversarial networks in inverse design (2025), [arXiv:2502.11934](https://arxiv.org/abs/2502.11934).
- [53] G. Huang, Z. Liu, L. van der Maaten, and K. Q. Weinberger, Densely Connected Convolutional Networks (2018), [arXiv:1608.06993](https://arxiv.org/abs/1608.06993).
- [54] S. Raza, M. Hammood, N. A. F. Jaeger, and L. Chrostowski, Fabrication-aware inverse design with shape optimization for photonic integrated circuits, *Opt. Lett.* **50**, 117 (2025).
- [55] R. P. Jenkins, S. D. Campbell, and D. H. Werner, Establishing exhaustive metasurface robustness against fabrication uncertainties through deep learning, *Nanophotonics* **10**, 4497 (2021).

Appendix A: Comparison to eigenmode simulations— Predictions made by physics-informed models operating according to the principle shown in schematic (1) are explainable in terms of the network-predicted physics parameters, which for the QNM-Net are $C(\omega)$, $\tilde{\omega}_m$, \mathbf{d}_m , and τ_m . Based on the theoretical foundations of the QNM expansion, we know that $\tilde{\omega}_m$ correspond exactly to eigen-

frequencies Maxwell's equations (2). Thus, the accuracy of the learned physics can be verified by comparing the network-predicted $\tilde{\omega}_m$ to eigenfrequencies calculated using full-wave eigenmode simulations. Figure 5 shows the network-predicted $\tilde{\omega}_1$ and the closest simulated eigenfrequency for 100 new randomly generated designs for the PhC slab example. The two methods closely agree, in-

dicating that the network training has converged to a representation of the spectra that matches the true underlying physics for this geometry.

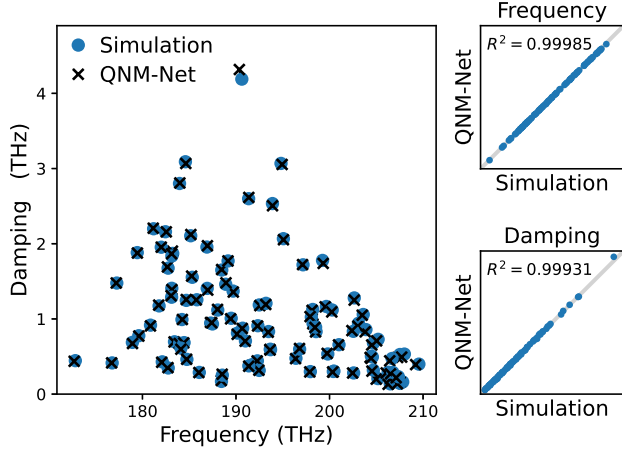


FIG. 5. Comparison between $\tilde{\omega}_1$ learned by the QNM-Net and calculated by full-wave eigenmode simulations for the PhC geometry. Left: QNM frequency and damping for 100 randomly generated designs. Right: Parity plots for frequency and damping with corresponding R^2 values.

More information about the physics could be discovered by investigating the other learned physics parameters. For example, if the symmetry of the mode had not already been included as a prior constraint in the PhC example, it could have been discovered by looking at the model predictions for \mathbf{d}_1 , which is proportional to $(1, 1)$ for an even mode.

Appendix B: Robustness to noise—The improved data efficiency of physics-informed approaches makes it feasible to train or fine-tune models on experimental data. Experimental data may contain design variations due to fabrication imperfections and random fluctuations in the measured spectra. We therefore investigate how the QNM-Net responds to noise in the data. The analysis was carried out for the PhC geometry with 160 training samples. Results are compared to a standard NN with 220k trainable parameters.

Figure 6 compares the QNM-Net and standard NN predictions on unseen samples with random perturbations added to all designs in the dataset before training. The accuracy of both models is adversely affected by the noise. Due to the physics constraints, the QNM-Net predicts spectra that are still physical, but with resonances shifted compared to the simulated result. The standard neural network instead predicts smoothed-out spectra, which may lead to lower S -MSE, but have unphysical resonance shapes.

Figure 7 shows QNM-Net and standard NN predictions on an unseen sample with increasing amounts of noise added to all spectra. The predictions of the QNM-

Net are essentially unaffected by the noise, because the

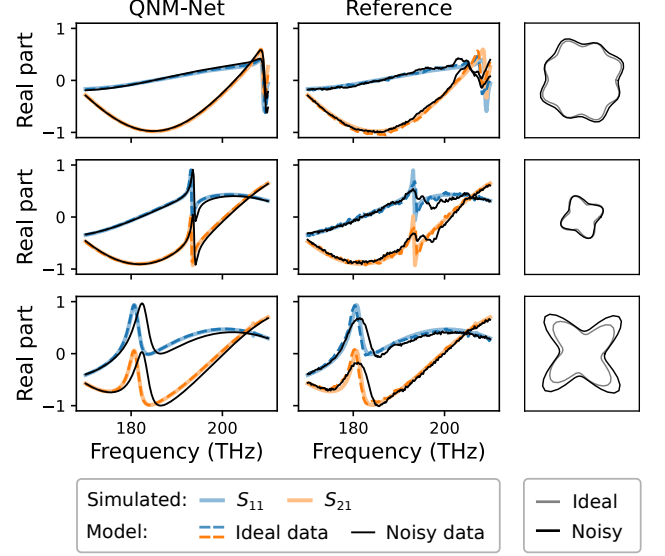


FIG. 6. Effect of design noise on model predictions. Left column: QNM-Net predictions for three unseen designs when trained with noise (black lines) and without noise (dashed lines) added to the data. Middle column: Corresponding standard NN predictions. Right column: Illustration of the PhC unit cell geometry.

noise cannot be represented within the constraints of the QNM expansion. The standard NN, on the other hand, is unable to separate noise from signal and, therefore, learns random fluctuations in the training data.

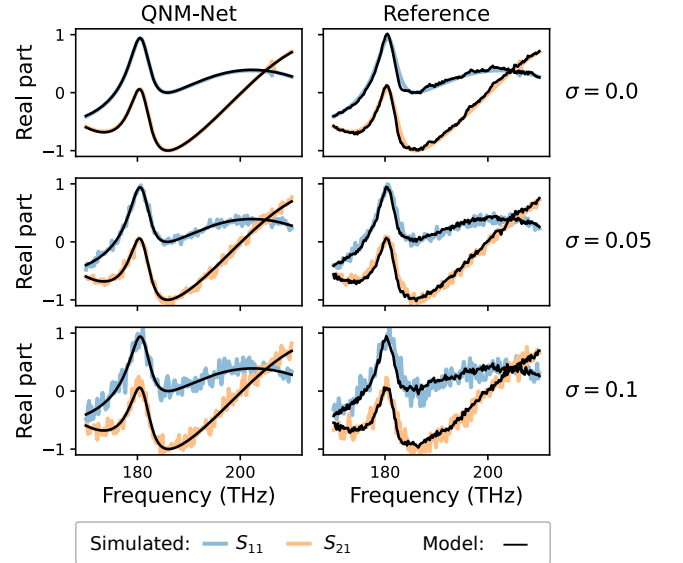


FIG. 7. Effect of spectrum noise on model predictions. Left column: QNM-Net predicted spectra (black lines) for an unseen sample with increasing amounts of noise added to the data. Right column: Corresponding standard NN predictions. The noise standard deviation σ is shown to the right.